AIMS Mathematics, 10(2): 3025–3040.
DOI: 10.3934/math.2025141
Received: 27 December 2024
Revised: 22 January 2025
Accepted: 10 February 2025
Published: 18 February 2025

https://www.aimspress.com/journal/Math

Research article

A study of dynamical features and novel soliton structures of complex-coupled Maccari's system

Naseem Abbas[1], **Amjad Hussain**[1,*], **Mohsen Bakouri**[2,3,*], **Thoraya N. Alharthi**[4] **and Ilyas Khan**[5,6,*]

[1] Department of Mathematics, Quaid-i-Azam University 45320, Islamabad 44000, Pakistan
[2] Department of Medical Equipment Technology, College of Applied Medical Science, Majmaah University, Majmaah 11952, Saudi Arabia
[3] Department of Physics, College of Arts, Fezzan University, Traghen 71340, Libya
[4] Department of Mathematics, College of Science, University of Bisha, P.O. Box 551, Bisha 61922, Saudi Arabia
[5] Department of Mathematics, College of Science Al-Zulfi, Majmaah University, Al-Majmaah 11952, Saudi Arabia
[6] Hourani Center for Applied Scientific Research, Al-Ahliyya Amman University, Amman, Jordan

* **Correspondence:** Email: a.hussain@qau.edu.pk, m.bakouri@mu.edu.sa, i.said@mu.edu.sa.

Abstract: This investigation focuses on solitary wave solutions and dynamic analysis of the complex coupled Maccari system. We employ the new extended hyperbolic function method to establish bright-wave and dark-wave profiles of the model. The resulting solutions include hyperbolic, trigonometric, and exponential-type functions. Furthermore, we explore the model's dynamical characteristics via multiple perspectives, including phase portrait analysis, quasi-periodic and chaotic patterns, sensitivity analysis and Lyapunov exponent. The analysis validates the robustness of the new extended hyperbolic function method on one hand and extends the understanding of complex wave structures in Maccari's system on the other hand.

Keywords: complex coupled Maccari system; nonlinear optics; soliton solutions; Chaos; bifurcation analysis and sensitivity
Mathematics Subject Classification: 35C08

1. Introduction

Maccari first obtained an integrable nonlinear system in 1996, hence the name of the nonlinear Maccari system (MS) in (2+1)-dimensions. The Maccari system is then found using an

asymptotically precise reduction method based on the Fourier expansion and spatio-temporal reformation of the Kadomtsev-Petviashvili equation [1]. Even though there isn't a single paradigm, researchers have looked at the nonlinear nature of rough waves in great detail through the lens of the (2+1)-dimensional nonlinear complex coupled Maccari (CCM) system [2]:

$$\begin{cases} iP_t + P_{xx} + PQ = 0, \\ Q_t + Q_y + (|P|^2)_x = 0, \end{cases} \tag{1.1}$$

where $i = \sqrt{-1}$, $P(x, y, t)$ and $Q(x, y, t)$ are the complex and real valued functions respectively. The lax pair of the Kadomtsev-Petviashvili equation is a clear sign of the integrability property that can be reached using the reduction strategy [3, 4]. Equation (1.1) explains the mobility of the solitary waves contained in a limiting area of space. Its implications for hydrodynamics, nonlinear optics, and especially plasma physics are equally noteworthy.

Many mathematical physics models admit soliton solutions [5], making the theory of optical solitons quite interesting. The observation of optical solitons is one of the key components of nonlinear fiber optics. Soliton has a variety of applications in engineering and applied science. Several mathematicians and physicists have studied the (2+1)-dimensional nonlinear complex-coupled Maccari system successfully. They have done this using various techniques, such as the $\exp(-\phi(\zeta))$-expansion method and the new (G'/G)-expansion method [6, 7]. Inç et al. [8] used the generalized projective Riccati equation technique and the extended F-expansion. Kumar and Chand [9] used the traveling wave reduction technique; Bulut et al. [10] used the modified trial equation method; Xu et al. [11] used the reduction of the KP hierarchy; and Neirameh [12] used the analytical method to find stationary wave solutions to the CCM system (1.1). In [13], the authors computed some exact traveling wave solutions to the same model using the Jacobi elliptic function method. The goal of this work is to find the novel exact traveling wave responses for the complex non-linear CCM system using a consistent method. Also, we show how the ranges of free parameters affect the wave structure of the responses that we find here.

Bifurcation analysis [14, 15] of dynamical systems has become a prominent field of study. It focuses on qualitative changes in system behavior due to small variations in parameters. Besides, analyzing chaos and the dynamics of nonlinear periodic waves is essential for understanding systems governed by differential equations. This research area is instrumental in comprehending the physical phenomena described by these equations, with some recent significant contributions noted in [16–19]. Vladimir Arnold's qualitative theory of differential equations [20] offers a robust framework for studying dynamical systems and detecting chaotic features. To fully understand chaotic dynamics, researchers use many different tools and methods, like Lyapunov exponents, Poincare visualizations, correlation integrals, Kolmogorov entropy analysis, time series assessment, chaos management, and fractal computation. In addition to the solitonic solutions, we also uncover the dynamical behavior of the CCM system using some of these tools. Note that in [21, 22], the authors have considered the complex structure (2+1) Maccari system. However, our system operates under the assumptions of simpler and localized dynamics.

The structure of the paper is as follows: In Section 2, the general description of the New Extended Hyperbolic Function Method is presented. The mathematical analysis and application of the method are described in Section 2.1. It performs a full dynamical analysis, looking at things like phase plane

analysis, chaotic behavior, and how sensitive the model is in Sections 3–5. The Lyapunov exponent is calculated for the model considered in Section 6. The concluding remarks are presented in Section 7.

2. The new extended hyperbolic function Method

The main steps of the new extended hyperbolic function method (EHFM) [23] are presented as follows: Consider a nonlinear partial differential equation of the form:

$$P(\Omega, \Omega_x, \Omega_t, \Omega_{xx}, \Omega_{xt}, \Omega_{tt}, \cdots) = 0, \tag{2.1}$$

where Ω be an indeterminate and P a function. Assume that P can be converted into an ODE using the following procedure:

$$O(U, U^{'}, U^{''}, ...) = 0, \;\; U^{'} = \frac{dU}{d\zeta}, \tag{2.2}$$

by taking into consideration $\Omega(x,t) = U(\zeta)e^{i(ax+bt+\omega)}$ where $\zeta = x - ct$. Assume for a moment that the non-trivial solution of Eq (2.2) may be written as:

Form 1

Using the wave transformation, the PDE in Eq (2.1) can be transformed into an ODE as shown in Eq (2.1). We assume that Eq (2.2) has a solution of the form:

$$U(\zeta) = \sum_{j=0}^{N} H_j S^j(\zeta), \tag{2.3}$$

where the coefficients H_j $(j = 1, 2, 3, \ldots, N)$ are constants to be determined, and $S(\zeta)$ satisfies the ODE:

$$\frac{dS}{d\zeta} = S\sqrt{A + BS^2}, \quad A, B \in \mathbb{R}. \tag{2.4}$$

By balancing the highest-order derivative and the highest power of the nonlinear term in Eq (2.1), the value of N is determined. Substituting Eq (2.3) into Eq (2.1) along with Eq (2.4) provides a system of algebraic equations for H_j $(j = 0, 1, 2, \ldots, N)$. Solving this system yields the following sets of solutions:

- **Set 1:** When $A > 0$ and $B > 0$,

$$S(\zeta) = -\sqrt{\frac{A}{B}}\,\mathrm{csch}\Big(\sqrt{A}(\zeta + \zeta_0)\Big). \tag{2.5}$$

- **Set 2:** When $A < 0$ and $B > 0$,

$$S(\zeta) = \sqrt{\frac{-A}{B}}\,\sec\Big(\sqrt{-A}(\zeta + \zeta_0)\Big). \tag{2.6}$$

- **Set 3:** When $A > 0$ and $B < 0$,

$$S(\zeta) = \sqrt{\frac{-A}{B}}\,\mathrm{sech}\Big(\sqrt{-A}(\zeta + \zeta_0)\Big). \tag{2.7}$$

- **Set 4:** When $A < 0$ and $B < 0$,

$$S(\zeta) = \sqrt{\frac{-A}{B}}\,\csc\Big(\sqrt{-A}(\zeta+\zeta_0)\Big). \tag{2.8}$$

- **Set 5:** When $A > 0$ and $B = 0$,

$$S(\zeta) = \exp\Big(\sqrt{A}(\zeta+\zeta_0)\Big). \tag{2.9}$$

- **Set 6:** When $A < 0$ and $B = 0$,

$$S(\zeta) = \cos\Big(\sqrt{-A}(\zeta+\zeta_0)\Big) + \iota\sin\Big(\sqrt{-A}(\zeta+\zeta_0)\Big). \tag{2.10}$$

- **Set 7:** When $A = 0$ and $B > 0$,

$$S(\zeta) = \pm\frac{1}{\sqrt{B}(\zeta+\zeta_0)}\cdot \tag{2.11}$$

- **Set 8:** When $A = 0$ and $B < 0$,

$$S(\zeta) = \pm\iota\sqrt{-B}(\zeta+\zeta_0). \tag{2.12}$$

Form 2

Similarly, assuming that $S(\zeta)$ satisfies the ODE:

$$\frac{dS}{d\zeta} = A + BS^2, \quad A, B \in \mathbb{R}, \tag{2.13}$$

we get a system of algebraic equations for H_j $(j = 1, 2, 3, \ldots, N)$. The solutions are:

- **Set 1:** When $AB > 0$,

$$S(\zeta) = \mathrm{sgn}(A)\sqrt{\frac{A}{B}}\,\tan\Big(\sqrt{AB}(\zeta+\zeta_0)\Big). \tag{2.14}$$

- **Set 2:** When $AB > 0$,

$$S(\zeta) = -\mathrm{sgn}(A)\sqrt{\frac{A}{B}}\,\cot\Big(\sqrt{AB}(\zeta+\zeta_0)\Big). \tag{2.15}$$

- **Set 3:** When $AB < 0$,

$$S(\zeta) = \mathrm{sgn}(A)\sqrt{\frac{-A}{B}}\,\tanh\Big(\sqrt{-AB}(\zeta+\zeta_0)\Big). \tag{2.16}$$

- **Set 4:** When $AB < 0$,

$$S(\zeta) = \mathrm{sgn}(A)\sqrt{\frac{-A}{B}}\,\coth\Big(\sqrt{-AB}(\zeta+\zeta_0)\Big). \tag{2.17}$$

- **Set 5:** When $A = 0$ and $B < 0$,

$$S(\zeta) = -\frac{1}{B(\zeta+\zeta_0)}\cdot \tag{2.18}$$

- **Set 6:** When $A = 0$ and $B > 0$,

$$S(\zeta) = B(\zeta+\zeta_0). \tag{2.19}$$

The symbol $\mathrm{sgn}(A)$ represents the signum function, which is defined as:

$$\mathrm{sgn}(A) = \begin{cases} 1, & \text{if } A > 0, \\ 0, & \text{if } A = 0, \\ -1, & \text{if } A < 0. \end{cases}$$

2.1. Application of the new EHFM

This part uses the new EHFM to find specific solutions for the non-linear CCM equations for the soliton. Putting the complex wave transformations

$$P(x, y, t) = e^{i\Theta}R(\rho), Q(x, y, t) = S(\rho)$$

where

$$\rho = x + y + \beta t, \Theta = a_1 x + a_2 y + a_3 t$$

into Eq (1.1) gives us the following nonlinear ordinary differential equations (NODEs):

$$\begin{cases} i(\beta + 2a_1)R' - (a_3 + a_1^2)R + R'' + RS = 0, \\ (1 + \beta)S' + 2RR' = 0, \end{cases} \tag{2.20}$$

where $\Theta = a_1 x + a_2 y + a_3 t$ and $\rho = x + y + \beta t$. The following results are obtained by separating both the first equation's imaginary as well as real parts in system (2.20):

$$\begin{cases} i(\beta + 2a_1)R' = 0, \\ -(a_3 + a_1^2)R + R'' + RS = 0. \end{cases} \tag{2.21}$$

From the first component of Eq (2.21), we obtain:

$$\beta = -2a_1. \tag{2.22}$$

Similarly by using above Eq (2.20)'s second component yields:

$$S = -\frac{1}{1 - 2a_1}R^2, \tag{2.23}$$

where the value of the integration constant is zero. Ultimately, by replacing the value of S given in Eq (2.23) into first half of Eq (2.20), we get the following NODE:

$$-(a_3 + a_1^2)(1 - 2a_1)R + (1 - 2a_1)R'' + R^3 = 0, \tag{2.24}$$

which after manipulation results in:

$$R'' = (a_3 + a_1^2)R - \frac{1}{(1 - 2a_1)}R^3. \tag{2.25}$$

After renaming the constants, we obtain

$$R'' = \sigma_1 R - \sigma_2 R^3, \tag{2.26}$$

where

$$\sigma_1 = (a_3 + a_1^2), \sigma_2 = \frac{1}{(1 - 2a_1)}.$$

Form 1

In this section, we apply the new EHFM for the solutions of the non-linear CCM equations. Utilizing balancing principal in Eq (2.24), gives $N = 1$. So, the Eq (2.3) reduces to

$$R(\rho) = H_0 + H_1 S(\rho), \tag{2.27}$$

where H_0 and H_1 are constants to be found. Substituting Eq (2.27) into Eq (2.24) and comparing the coefficients of each polynomial of $S(\rho)$ to zero, we get a set of algebraic equations in H_0, H_1, A and B.

$$A = a_1^2 + a_3, \quad H_0 = 0, \quad H_1 = \sqrt{2B}\sqrt{2a_1 - 1}, \quad B = B. \tag{2.28}$$

- **Set 1:** When $A > 0$ and $B > 0$,

$$\begin{cases} P_9(x,y,t) = -\sqrt{2B}\sqrt{2a_1-1}\sqrt{\frac{a_1^2+a_3}{B}}\operatorname{csch}\left(\sqrt{a_1^2+a_3}(\rho+\rho_0)\right)e^{i(a_1x+a_2y+a_3t)}, \\ Q_9(x,y,t) = \frac{1}{1-2a_1}\left(\sqrt{2B}\sqrt{2a_1-1}\sqrt{\frac{a_1^2+a_3}{B}}\operatorname{csch}\left(\sqrt{a_1^2+a_3}(\rho+\rho_0)\right)\right)^2. \end{cases} \tag{2.29}$$

  where $\rho = x + y + \beta t$.
- **Set 2:** When $A < 0$ and $B > 0$,

$$\begin{cases} P_{10}(x,y,t) = \sqrt{2B}\sqrt{2a_1-1}\sqrt{\frac{-(a_1^2+a_3)}{B}}\sec\left(\sqrt{-(a_1^2+a_3)}(\rho+\rho_0)\right)e^{i(a_1x+a_2y+a_3t)}, \\ Q_{10}(x,y,t) = \frac{1}{1-2a_1}\left(\sqrt{2B}\sqrt{2a_1-1}\sqrt{\frac{-(a_1^2+a_3)}{B}}\sec\left(\sqrt{-(a_1^2+a_3)}(\rho+\rho_0)\right)\right)^2. \end{cases} \tag{2.30}$$

  where $\rho = x + y + \beta t$.
- **Set 3:** When $A > 0$ and $B < 0$,

$$\begin{cases} P_{11}(x,y,t) = \sqrt{2B}\sqrt{2a_1-1}\sqrt{\frac{-(a_1^2+a_3)}{B}}\operatorname{sech}\left(\sqrt{-(a_1^2+a_3)}(\rho+\rho_0)\right)e^{i(a_1x+a_2y+a_3t)}, \\ Q_{11}(x,y,t) = \frac{1}{1-2a_1}\left(\sqrt{2B}\sqrt{2a_1-1}\sqrt{\frac{-(a_1^2+a_3)}{B}}\operatorname{sech}\left(\sqrt{-(a_1^2+a_3)}(\rho+\rho_0)\right)\right)^2. \end{cases} \tag{2.31}$$

  where $\rho = x + y + \beta t$.
- **Set 4:** When $A < 0$ and $B < 0$,

$$\begin{cases} P_{12}(x,y,t) = \sqrt{2B}\sqrt{2a_1-1}\sqrt{\frac{-(a_1^2+a_3)}{B}}\csc\left(\sqrt{-(a_1^2+a_3)}(\rho+\rho_0)\right)e^{i(a_1x+a_2y+a_3t)}, \\ Q_{12}(x,y,t) = \frac{1}{1-2a_1}\left(\sqrt{2B}\sqrt{2a_1-1}\sqrt{\frac{-(a_1^2+a_3)}{B}}\csc\left(\sqrt{-(a_1^2+a_3)}(\rho+\rho_0)\right)\right)^2. \end{cases} \tag{2.32}$$

  where $\rho = x + y + \beta t$.
- **Set 5:** When $A > 0$ and $B = 0$,

$$\begin{cases} P_{13}(x,y,t) = \sqrt{2B}\sqrt{2a_1-1}\exp\left(\sqrt{(a_1^2+a_3)}(\rho+\rho_0)\right)e^{i(a_1x+a_2y+a_3t)}, \\ Q_{13}(x,y,t) = \frac{1}{1-2a_1}\left(\sqrt{2B}\sqrt{2a_1-1}\exp\left(\sqrt{(a_1^2+a_3)}(\rho+\rho_0)\right)\right)^2. \end{cases} \tag{2.33}$$

  where $\rho = x + y + \beta t$.

- **Set 6:** When $A < 0$ and $B = 0$,

$$\begin{cases} P_{14}(x,y,t) = \sqrt{2B}\sqrt{2a_1-1}\Big[\cos\Big(\sqrt{-(a_1^2+a_3)}(\rho+\rho_0)\Big) \\ +\sin\Big(\sqrt{-(a_1^2+a_3)}(\rho+\rho_0)\Big)\Big]e^{i(a_1x+a_2y+a_3t)}, \\ Q_{14}(x,y,t) = \frac{1}{1-2a_1}\Big(\cos\Big(\sqrt{-(a_1^2+a_3)}(\rho+\rho_0)\Big) + \sin\Big(\sqrt{-(a_1^2+a_3)}(\rho+\rho_0)\Big)\Big)^2. \end{cases} \tag{2.34}$$

  where $\rho = x + y + \beta t$.
- **Set 7:** When $A = 0$ and $B > 0$,

$$\begin{cases} P_{15}(x,y,t) = \sqrt{2B}\sqrt{2a_1-1}\left[\pm\frac{1}{\sqrt{B}(\rho+\rho_0)}\right]e^{i(a_1x+a_2y+a_3t)}, \\ Q_{15}(x,y,t) = \frac{1}{1-2a_1}\left(\sqrt{2B}\sqrt{2a_1-1}\left[\pm\frac{1}{\sqrt{B}(\rho+\rho_0)}\right]\right)^2. \end{cases} \tag{2.35}$$

  where $\rho = x + y + \beta t$.
- **Set 8:** When $A = 0$ and $B < 0$,

$$\begin{cases} P_{16}(x,y,t) = \sqrt{2B}\sqrt{2a_1-1}\left[\pm\iota\sqrt{-B}(\rho+\rho_0)\right]e^{i(a_1x+a_2y+a_3t)}, \\ Q_{16}(x,y,t) = \frac{1}{1-2a_1}\left(\sqrt{2B}\sqrt{2a_1-1}\left[\pm\iota\sqrt{-B}(\rho+\rho_0)\right]\right)^2. \end{cases} \tag{2.36}$$

Form 2

Utilizing balancing principal in Eq (2.24), gives $N = 1$. So, Eq (2.3) reduces to

$$R(\rho) = H_0 + H_1 S(\rho), \tag{2.37}$$

where H_0 and H_1 are constants to be found. Substituting Eq (2.37) into Eq (2.24) and comparing the coefficients of each polynomial of $S(\rho)$ to zero, we get a set of algebraic equations in H_0, H_1, A and B. Solving the set of equations, we get

$$B = \frac{1}{2A}(a_1^2+a_3), \quad H_0 = 0, \quad H_1 = \frac{(a_1^2+a_3)}{A}\sqrt{-\frac{1}{2}+a_1}, \quad A = A. \tag{2.38}$$

- **Set 1:** When $AB > 0$,

$$\begin{cases} P_{17}(x,y,t) = \frac{(a_1^2+a_3)}{A}\sqrt{-\frac{1}{2}+a_1}\sqrt{\frac{2A^2}{(a_1^2+a_3)}}\tan\Big(\sqrt{\frac{1}{2}(a_1^2+a_3)}(\rho+\rho_0)\Big)e^{i(a_1x+a_2y+a_3t)}, \\ Q_{17}(x,y,t) = \frac{1}{1-2a_1}\left(\frac{(a_1^2+a_3)}{A}\sqrt{-\frac{1}{2}+a_1}\sqrt{\frac{2A^2}{(a_1^2+a_3)}}\tan\Big(\sqrt{\frac{1}{2}(a_1^2+a_3)}(\rho+\rho_0)\Big)\right)^2. \end{cases} \tag{2.39}$$

  where $\rho = x + y + \beta t$.
- **Set 2:** When $AB > 0$,

$$\begin{cases} P_{18}(x,y,t) = \frac{(a_1^2+a_3)}{A}\sqrt{-\frac{1}{2}+a_1}\sqrt{\frac{2A^2}{(a_1^2+a_3)}}\cot\Big(\sqrt{\frac{1}{2}(a_1^2+a_3)}(\rho+\rho_0)\Big)e^{i(a_1x+a_2y+a_3t)}, \\ Q_{18}(x,y,t) = \frac{1}{1-2a_1}\left(\frac{(a_1^2+a_3)}{A}\sqrt{-\frac{1}{2}+a_1}\sqrt{\frac{2A^2}{(a_1^2+a_3)}}\cot\Big(\sqrt{\frac{1}{2}(a_1^2+a_3)}(\rho+\rho_0)\Big)\right)^2. \end{cases} \tag{2.40}$$

  where $\rho = x + y + \beta t$.

- **Set 3:** When $AB < 0$,

$$\begin{cases} P_{19}(x,y,t) = \frac{(a_1^2+a_3)}{A}\sqrt{-\frac{1}{2}+a_1}\sqrt{\frac{-2A^2}{(a_1^2+a_3)}}\tanh\left(\sqrt{\frac{-1}{2}(a_1^2+a_3)}(\rho+\rho_0)\right)e^{i(a_1x+a_2y+a_3t)}, \\ Q_{19}(x,y,t) = \frac{1}{1-2a_1}\left(\frac{(a_1^2+a_3)}{A}\sqrt{-\frac{1}{2}+a_1}\sqrt{\frac{-2A^2}{(a_1^2+a_3)}}\tanh\left(\sqrt{\frac{-1}{2}(a_1^2+a_3)}(\rho+\rho_0)\right)\right)^2. \end{cases} \tag{2.41}$$

  where $\rho = x + y + \beta t$.

- **Set 4:** When $AB < 0$,

$$\begin{cases} P_{20}(x,y,t) = \frac{(a_1^2+a_3)}{A}\sqrt{-\frac{1}{2}+a_1}\sqrt{\frac{-2A^2}{(a_1^2+a_3)}}\coth\left(\sqrt{\frac{-1}{2}(a_1^2+a_3)}(\rho+\rho_0)\right)e^{i(a_1x+a_2y+a_3t)}, \\ Q_{20}(x,y,t) = \frac{1}{1-2a_1}\left(\frac{(a_1^2+a_3)}{A}\sqrt{-\frac{1}{2}+a_1}\sqrt{\frac{-2A^2}{(a_1^2+a_3)}}\coth\left(\sqrt{\frac{-1}{2}(a_1^2+a_3)}(\rho+\rho_0)\right)\right)^2. \end{cases} \tag{2.42}$$

  where $\rho = x + y + \beta t$.

- **Set 5:** When $A = 0$ and $B < 0$,

$$\begin{cases} P_{21}(x,y,t) = \frac{(a_1^2+a_3)}{A}\sqrt{-\frac{1}{2}+a_1}\left[-\frac{2A}{(a_1^2+a_3)(\rho+\rho_0)}\right]e^{i(a_1x+a_2y+a_3t)}, \\ Q_{21}(x,y,t) = \frac{1}{1-2a_1}\left(\frac{(a_1^2+a_3)}{A}\sqrt{-\frac{1}{2}+a_1}\left[-\frac{2A}{(a_1^2+a_3)(\rho+\rho_0)}\right]\right)^2. \end{cases} \tag{2.43}$$

  where $\rho = x + y + \beta t$.

- **Set 6:** When $A = 0$ and $B > 0$,

$$\begin{cases} P_{22}(x,y,t) = \frac{(a_1^2+a_3)}{A}\sqrt{-\frac{1}{2}+a_1}\left[\frac{1}{2A}(a_1^2+a_3)(\rho+\rho_0)\right]e^{i(a_1x+a_2y+a_3t)}, \\ Q_{22}(x,y,t) = \frac{1}{1-2a_1}\left(\frac{(a_1^2+a_3)}{A}\sqrt{-\frac{1}{2}+a_1}\left[\frac{1}{2A}(a_1^2+a_3)(\rho+\rho_0)\right]\right)^2. \end{cases} \tag{2.44}$$

  where $\rho = x + y + \beta t$.

The physical interpretation of these figures, based on their descriptions and visualization, relates to bright solitons (Figures 1, 4) and dark solitons (Figures 2, 3). These solitons are localized wave solutions in nonlinear systems that maintain their shape while propagating due to a balance between dispersion and nonlinearity.

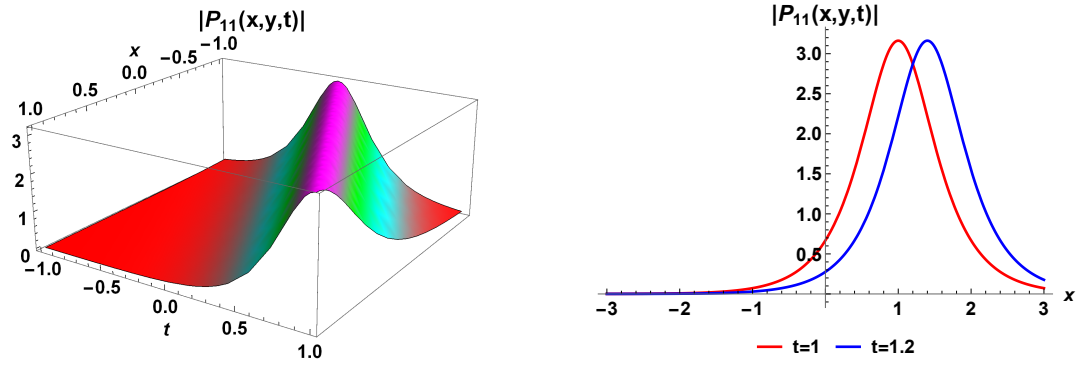

(a) 3D-plot **(b)** 2D-plot

Figure 1. Bright soliton solution view of the $P_{11}(x,y,t)$ with parameters $B = 4$, $a_1 = 1.0$, $a_2 = 1$, $a_3 = 2$ and $\beta = 2$.

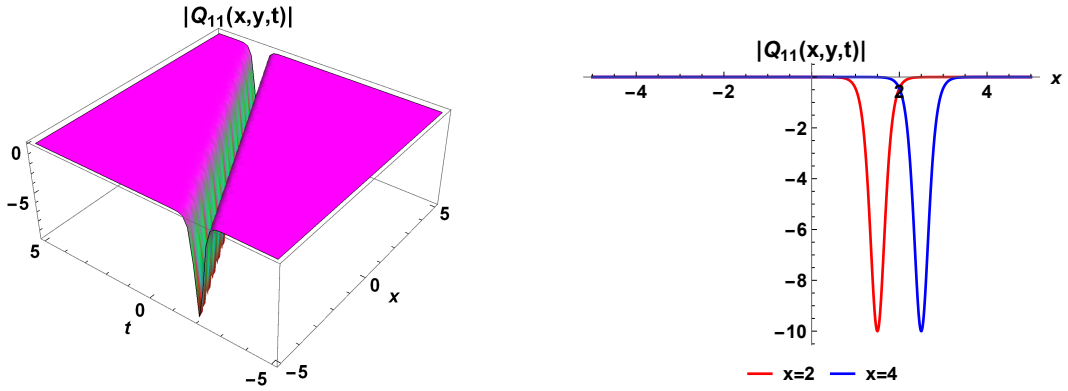

(a) 3D-plot **(b)** 2D-plot

Figure 2. Dark soliton solution view of the $Q_{11}(x, y, t)$ with parameters $B = 4$, $a_1 = 1.0$, $a_2 = 1$, $a_3 = 2$ and $\beta = 2$.

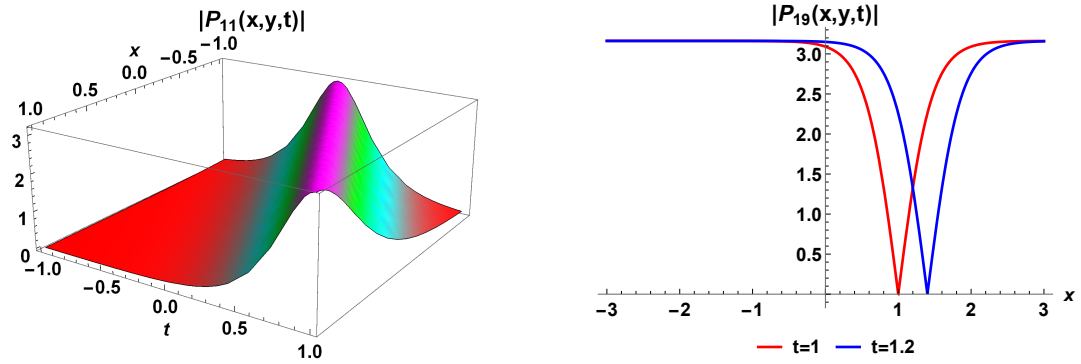

(a) 3D-plot **(b)** 2D-plot

Figure 3. Dark soliton solution view of the $P_{19}(x, y, t)$ with parameters $B = 4$, $a_1 = 4.0$, $a_2 = 2$, $a_3 = 1$ and $\beta = 3$.

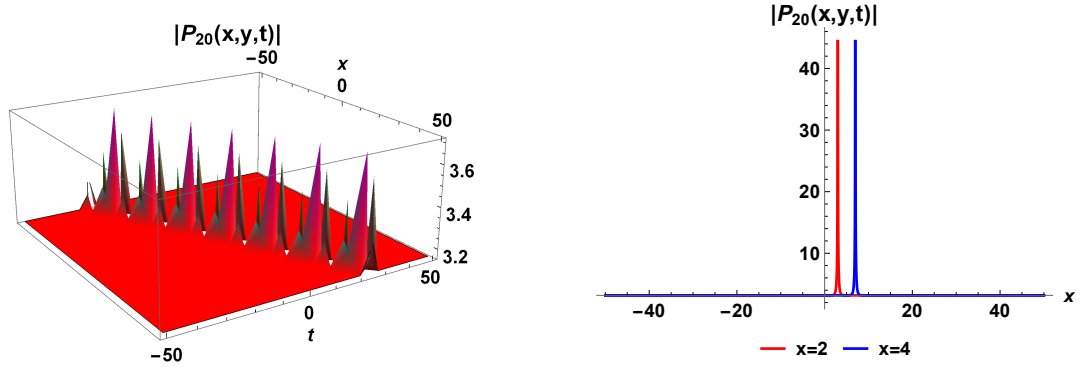

(a) 3D-plot **(b)** 2D-plot

Figure 4. Bright soliton solution view of the $P_{20}(x, y, t)$ with parameters $B = 4$, $a_1 = 1.0$, $a_2 = 1$, $a_3 = 2$ and $\beta = 2$.

3. Phase-plane analysis

Phase plane analysis is the main emphasis of this section's in-depth examination of Eq (1.1). Assuming $R' = S$ as the Galilean transformation, we get a planar dynamical system of the following type:

$$\begin{cases} \frac{dR}{dt} = S, \\ \frac{dS}{dt} = \sigma_1 R - \sigma_2 R^3, \end{cases} \tag{3.1}$$

where the values of σ_1 and σ_2 are listed above. Given that system (3.1) is the first integral Hamiltonian [24]

$$H(R, S) = \frac{\sigma_1 R^2}{2} - \frac{\sigma_2 R^4}{4} - \frac{S^2}{2} = \hat{g}, \tag{3.2}$$

where the Hamiltonian constant is $\hat{g}$. The capacity of the Hamiltonian function to give a clear and comprehensive explanation for the overall energy dynamics of a physical phenomenon accounts for its prominence. It is fundamental to both classical and quantum physics, allowing for the creation of equations of motion and long-term system behavior predictions. Additionally, the advancement of analytical as well as computational techniques for researching and modeling physical structures depends heavily upon the Hamiltonian. A vector field for system (3.1) constrains the planar dynamical system's phase trajectories. Consequently, we must examine many system phase profiles (3.1) with varying parameter configurations. Three equilibrium points exist for the system (3.1) about the non-zero components σ_1 and σ_2.

$$P_1 = (0, 0), \quad P_2 = (\sqrt{\frac{\sigma_1}{\sigma_2}}, 0), \quad P_3 = (-\sqrt{\frac{\sigma_1}{\sigma_2}}, 0). \tag{3.3}$$

$$J(R, S) = \det\begin{pmatrix} 0 & 1 \\ \sigma_1 - 3\sigma_2 R^2 & 0 \end{pmatrix} = -\sigma_1 + 3\sigma_2 R^2. \tag{3.4}$$

As a saddle point of $J(R, S) < 0$, a centre of $J(R, S) > 0$, and a cuspidal location of $J(R, S) = 0$, referred to as state point $(P_i, 0)$, $i = 1, 2, 3$ is identified. We consider many scenarios for the parameters involved in the dynamical system (3.1) to examine the phase plane assessment of the system. Regarding system (3.1), phase patterns are shown in Figures 5 and 6.

Case 1: Whenever both $\sigma_1 > 0$ and $\sigma_2 > 0$. Three distinct equilibrium points $P_1 = (0, 0), P_2 = (1, 0)$, and $P_3 = (-1, 0)$ have been produced and are depicted in Figure 5(a) by taking into consideration different values of the related constants, such as $a_1 = 1, a_3 = -2$ and $-2a_1 = 0.001$. The image makes it evident that there P_1 is a saddle point in addition to P_2 and P_3 are center points.
Case 2: $\sigma_1 < 0$ and $\sigma_2 < 0$, if that is. Three distinct equilibrium points, $P_1 = (0, 0), P_2 = (1, 0)$, and $P_3 = (-1, 0)$, have been found by taking into account various values of the relevant constants, such as $a_1 = 1, a_3 = -2$ and $-2a_1 = -2$. These are shown in Figure 5(b)). The image makes it evident that P_1 is a center point and that P_2 and P_3 are saddle points.
Case 3: Assuming $\sigma_2 < 0$ and $\sigma_1 > 0$. Three distinct equilibrium stages, $P_1 = (0, 0), P_2 = (i, 0)$ and $P_3 = (-i, 0)$, were found by taking into account various values of the relevant constants, such as $a_1 = 2, a_3 = 3$, and $-2a_1 = -2$. One genuine point is depicted in Figure 6(a). The illustration makes it

very evident that P_1 represents a saddle position.

Case 4: Assuming that $\sigma_1 < 0$ and $\sigma_2 > 0$. Three distinct equilibrium indications, $P_1 = (0, 0), P_2 = (i, 0)$ and $P_3 = (-i, 0)$, were successfully found by taking into account various values of the relevant constants, such as $a_1 = 1, a_3 = -2$ as well as $-2a_1 = 0.0001$. One genuine point is depicted in Figure 6(b). The image makes it very evident whether P_1 is a central point.

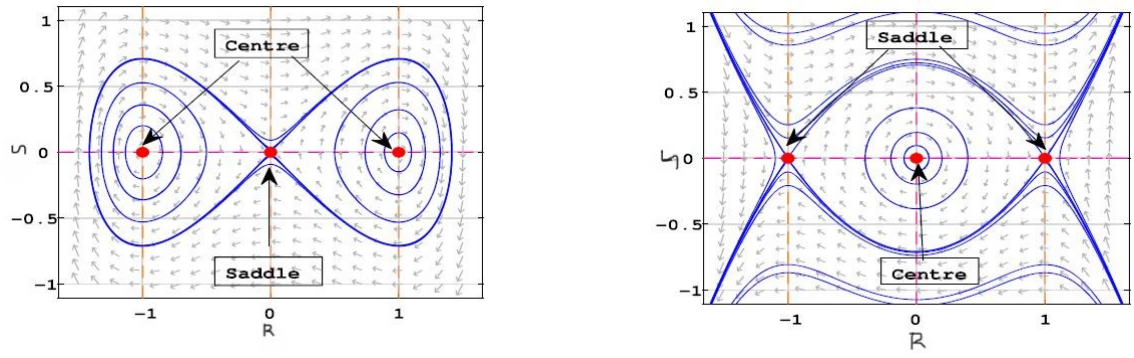

(a) $\sigma_1 > 0$ and $\sigma_2 > 0$ **(b)** $\sigma_1 < 0$ and $\sigma_2 < 0$

Figure 5. Phase portrait analysis of system (3.1).

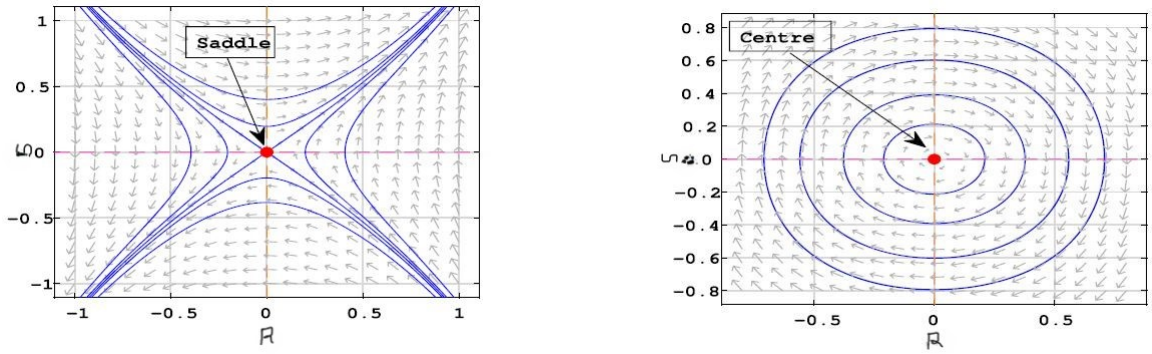

(a) $\sigma_1 > 0$ and $\sigma_2 < 0$ **(b)** $\sigma_1 < 0$ and $\sigma_2 > 0$

Figure 6. Phase portrait analysis of system (3.1).

4. Quasi-periodic activities

This section involves analyzing the quasi-periodic pattern [14] of the model under consideration with the addition of an exterior perturbation factor to the planar dynamical structure (3.1). Next, we can compose

$$\begin{cases} \frac{dR}{dt} = S, \\ \frac{dS}{dt} = \sigma_1 R - \sigma_2 R^3 + p_0 \cos(q_0 t), \end{cases} \tag{4.1}$$

where the amplitude and frequency of the external perturbation term applied to the system (3.1) are indicated by the variables p_0 and q_0. This evaluation illustrates how the characteristics of a planar

dynamical system (3.1) are affected by an external perturbation force. To do this, we alter the values of p_0 and q_0 while fixing all other system (4.1) parameters. Figures 7 and 8 Slight modifications to the external force's frequency and magnitude can be used to show how a certain model behaves quasi-periodically when its solution gets out of control. The quasi-periodic behavior of a dynamical system exhibits disrupted periodic patterns. A quasi-periodic behavior exhibits some regularity or repetitive pattern, but the period may not be constant. The cosine function is commonly used to capture the oscillatory behavior due to its mathematical properties. The choice of using the cosine function for quasi-periodic patterns is somewhat arbitrary, it has proven to be useful in various fields such as physics and engineering.

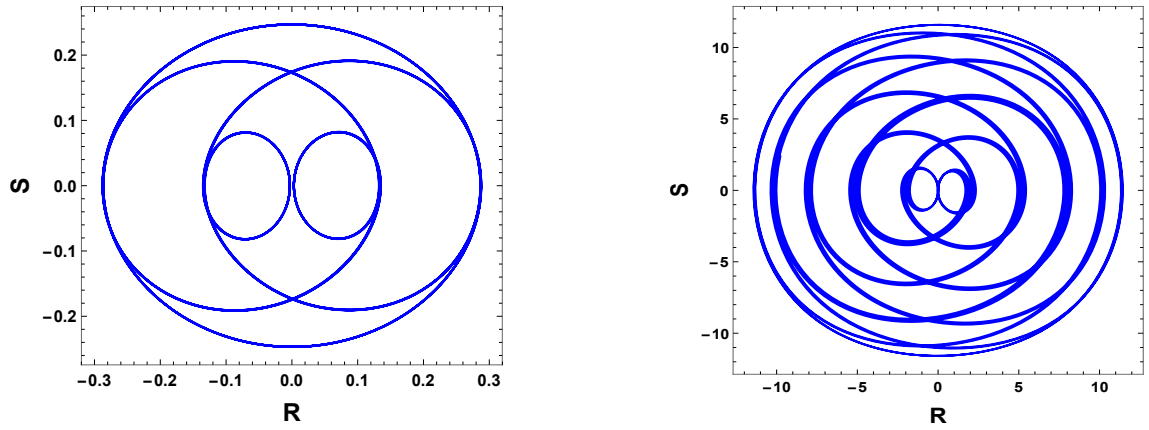

(a) $p_0 = 0.1$ and $q_0 = 0.6$. **(b)** $p_0 = 2.01$ and $q_0 = 0.9$

Figure 7. Effect of p_0 and q_0 on the system (4.1).

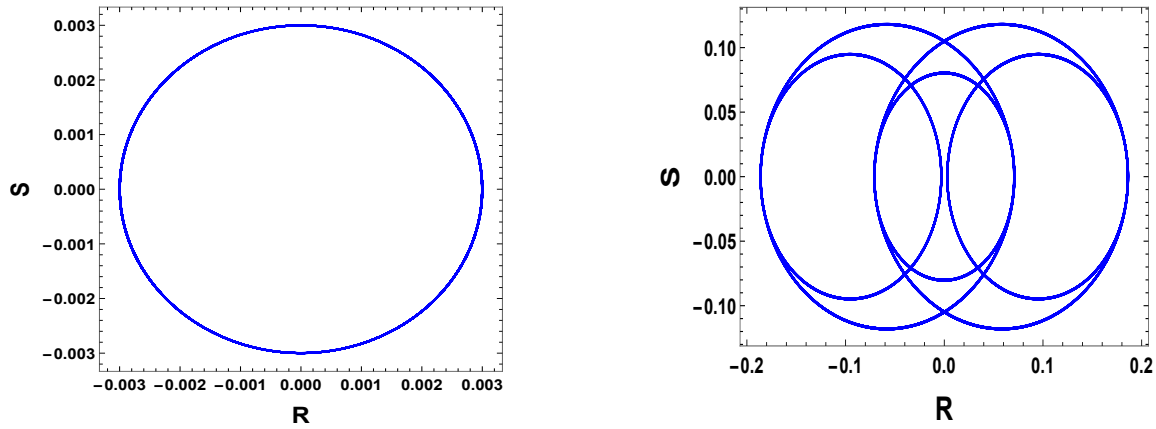

(a) $p_0 = 0.0$ and $q_0 = 0.9$. **(b)** $p_0 = 0.1$ and $q_0 = 0.2$

Figure 8. Effect of p_0 and q_0 on the system (4.1).

5. Sensitivity to the initial conditions

The chosen model's sensitivity is explained in this section. Sensitivity analysis is a method used to ascertain how changes to the model's parameters or inputs impact the problem's outcomes. Sensitivity

analysis can be used to evaluate how changes to physical properties or situations affect a system's behavior in terms of physical impacts. One aspect of chaos is its sensitivity to the initial conditions. Here we used the Runge-Kutta 4th Order Method (RK4) to perform sensitivity analysis to study how a nonlinear system responds to small changes in its initial conditions. This numerical method provides highly accurate solutions to ordinary differential equations, allowing us to calculate and compare system trajectories for slightly perturbed initial conditions. By observing whether these trajectories diverge or converge, we can assess the sensitivity of the system. The RK4 method is particularly suitable for this purpose due to its precision and reliability in capturing the behavior of nonlinear systems. The sensitivity to the initial conditions can be seen in Figures 9 and 10, which may be viewed as chaotic.

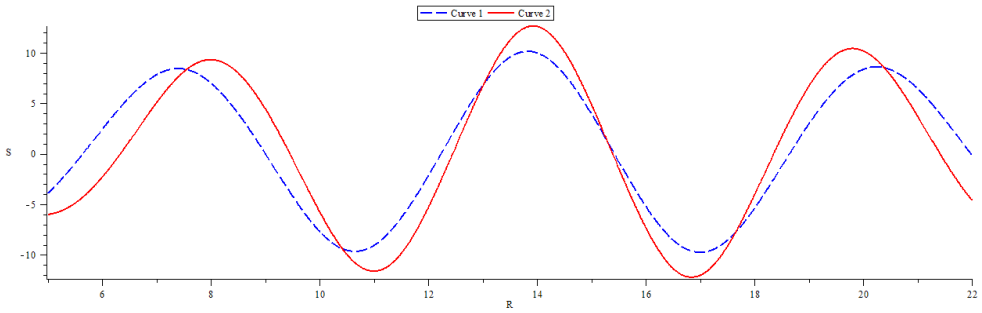

Figure 9. Sensitivity map for system (4.1) assuming initial conditions $(1.1, 0.1)$ and $(5.5, 0.5)$ for curves 1 and 2, accordingly, and $\sigma_1 = -1, \sigma_2 = 0.003, p_0 = 2.5, q_0 = 0.91$.

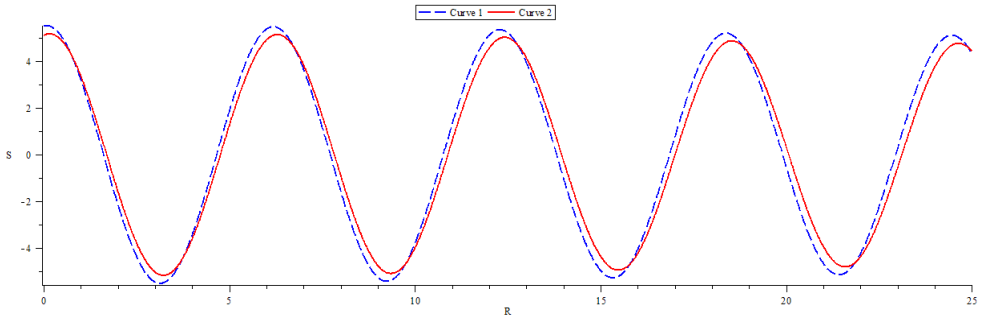

Figure 10. Sensitivity map for system (4.1) assuming initial conditions $(5.1, 0.9)$ as well as $(5.5, 0.52)$ for contours 1 and 2, corresponding to $\sigma_1 = -1, \sigma_2 = 0.003, p_0 = 0.05, q_0 = 0.91$.

6. Lyapunov exponent

This section explores the behavior of the Lyapunov exponent of the proposed model. System (4.1), including the perturbation term, can be expressed in an autonomous form as follows:

$$\begin{cases} \frac{dR}{dt} = S, \\ \frac{dS}{dt} = \sigma_1 R - \sigma_2 R^3 + p_0 \cos(z), \\ \frac{dz}{dt} = q_0, \end{cases} \tag{6.1}$$

where $z = q_0 t$. The Lyapunov exponent quantifies how rapidly nearby trajectories in a dynamical system diverge, serving as an indicator of the system's chaotic tendencies. A positive Lyapunov

exponent implies chaotic behavior, while a negative value denotes system stability. The magnitude of the exponent is proportional to the rate of divergence, with higher values suggesting increased chaos. We calculated the Lyapunov exponents for system (6.1) and depicted their evolution over time. Figure 11 presents the Lyapunov exponents as a function of time for the perturbed system with suitable parameter values.

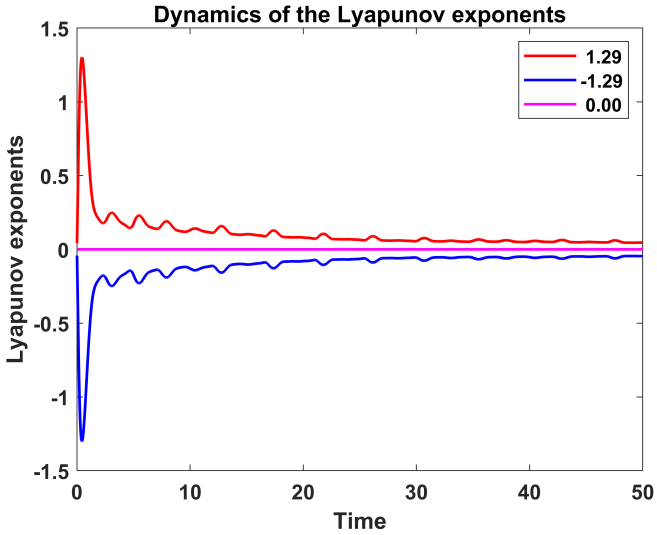

Figure 11. Lyapunov Exponent for system (4.1) assuming initial conditions $(0.9, 0.9, 0.9)$ corresponding to $\sigma_1 = -1$, $\sigma_2 = 1$, $p_0 = 0.0$, $q_0 = 0.1$.

7. Conclusions

The new extended hyperbolic function method computes analytical solutions for the mathematical model of complex-coupled Maccari's system, yielding solutions for hyperbolic, trigonometric, and exponential functions. Both bright and dark-shaped solutions are among the outcomes. The dynamical analysis reveals attractor chaos in the complex coupled Maccari structure, a result of traveling wave solutions occurring at various locations and closely linked to the equilibrium point. The established bifurcation, in conjunction with chaos theory, enhances researchers' understanding of the system's behavior, enabling more precise predictive modeling. Furthermore, by applying ideas from chaos, including bifurcation theory, we can design functional control systems. These findings have several applications that will progress in design, control, forecasting, and optimization.

Author contributions

Naseem Abbas: Writing original draft, Software, Methodology, Formal analysis; Amjad Hussain: Writing review and editing, Visualization, Validation, Supervision; Mohsen Bakouri: Investigation, Formal analysis, Conceptualization; Thoraya N. Alharthi: Visualization, Validation, Supervision; Ilyas Khan: Methodology, Analysis, Writing review and editing, Supervision; Ilyas Khan: Investigation, Formal analysis, Conceptualization. All authors have read and approved the final version of the manuscript for publication.

Use of Generative-AI tools declaration

The authors declare that they have not used Artificial Intelligence (AI) tools in the creation of this article.

Acknowledgments

The author Mohsen Bakouri extends the appreciation to the Deanship of Postgraduate Studies and Scientific Research at Majmaah University for funding this research work through the project number R-2025-1589.

Conflict of interest

The authors declare that they have no conflict of interest.

References

1. S. Zhang, Exp-function method for solving Maccari's system, *Phys. Lett. A*, **371** (2007), 65–71. https://doi.org/10.1016/j.physleta.2007.05.091
2. S. Y. Arafat, K. Fatema, M. E. Islam, M. A. Akbar, Promulgation on various genres soliton of Maccari system in nonlinear optics, *Opt. Quant. Electron.*, **54** (2022), 206. https://doi.org/10.1007/s11082-022-03576-0
3. A. Maccari, The Kadomtsev-Petviashvili equation as a source of integrable model equations, *J. Math. Phys.*, **37** (1996), 6207–6212. https://doi.org/10.1063/1.531773
4. N. Cheemaa, S. Chen, A. R. Seadawy, Propagation of isolated waves of coupled nonlinear (2+1)-dimensional Maccari system in plasma physics, *Results Phys.*, **17** (2020), 102987. https://doi.org/10.1016/j.rinp.2020.102987
5. R. Ali, D. Kumar, A. Akgul, A. Altalbe, On the periodic soliton solutions for fractional Schrodinger equations, *Fractals*, **32** (2024), 2440033. https://doi.org/10.1142/S0218348X24400334
6. M. G. Hafez, M. N. Alam, M. A. Akbar, Traveling wave solutions for some important coupled nonlinear physical models via the coupled Higgs equation and the Maccari system, *J. King Saud Uni. Sci.*, **27** (2015), 105–112. https://doi.org/10.1016/j.jksus.2014.09.001
7. M. G. Hafez, B. Zheng, M. A. Akbar, Exact travelling wave solutions of the coupled nonlinear evolution equation via the Maccari system using novel $(G^{'}/G)$-expansion method, *Egypt. J. Basic Appl. Sci.*, **2** (2015), 206–220. https://doi.org/10.1016/j.ejbas.2015.04.002
8. M. Inc, A. I. Aliyu, A. Yusuf, D. Baleanu, E. Nuray, Complexiton and solitary wave solutions of the coupled nonlinear Maccari's system using two integration schemes, *Modern Phys. Lett. B*, **32** (2018), 1850014. https://doi.org/10.1142/S0217984918500148
9. H. Kumar, F. Chand, Exact traveling wave solutions of some nonlinear evolution equations, *J. Theor. Appl. Phys.*, **8** (2014), 114. https://doi.org/10.1007/s40094-014-0114-z
10. H. Bulut, G. Yel, H. M. Baskonus, Novel structure to the coupled nonlinear Maccari's system by using modified trial equation method, *Adv. Math. Models Appl.*, **2** (2017), 14–19.

11. T. Xu, Y. Chen, Z. Qiao, Multi-dark soliton solutions for the (2+1)-dimensional multi-component Maccari system, *Modern Phys. Lett. B*, **33**, (2019), 1950390. https://doi.org/10.1142/S0217984919503901
12. A. Neirameh, New analytical solutions for the coupled nonlinear Maccari's system, *Alex. Eng. J.*, **55** (2016), 2839–2847. https://doi.org/10.1016/j.aej.2016.07.007
13. N. Cheemaa, M. Younis, New and more exact traveling wave solutions to integrable (2+1)-dimensional Maccari system, *Nonlinear Dyn.*, **83** (2016), 1395–1401. https://doi.org/10.1007/s11071-015-2411-8
14. A. Saha, S. Banerjee, *Dynamical systems and nonlinear waves in plasmas*, New York: CRC Press, 2021. https://doi.org/10.1201/9781003042549
15. N. K. Pal, P. Chatterjee, A. Saha, Solitons, multi-solitons and multi-periodic solutions of the generalized Lax equation by Darboux transformation and its quasiperiodic motions, *Int. J. Modern Phys. B*, **38** (2023), 2440001. https://doi.org/10.1142/S0217979224400010
16. A. Jhangeer, W. A. Faridi, M. Alshehri, Soliton wave profiles and dynamical analysis of fractional Ivancevic option pricing model, *Sci. Rep.*, **14** (2024), 23804. https://doi.org/10.1038/s41598-024-74770-1
17. N. Abbas, A. Hussain, Novel soliton structures and dynamical behaviour of coupled Higgs field equations, *Eur. Phys. J. Plus*, **139** (2024), 327. https://doi.org/10.1140/epjp/s13360-024-05124-z
18. A. Hussain, N. Abbas, S. Niazai, I. Khan, Dynamical behavior of Lakshamanan-Porsezian-Daniel model with spatiotemporal dispersion effects, *Alex. Eng. J.*, **96**, (2024), 332–343. https://doi.org/10.1016/j.aej.2024.03.024
19. A. Hussain, N. Abbas, Periodic, quasi-periodic, chaotic waves and solitonic structures of coupled Benjamin-Bona-Mahony-KdV system, *Phys. Scr.*, **99** (2024), 125231. https://doi.org/10.1088/1402-4896/ad896b
20. V. I. Arnold, *Ordinary differential equations*, Berlin: Springer Science & Business Media, 1992.
21. R. Ali, E. Tag-eldin, A comparative analysis of generalized and extended (G'/G)-Expansion methods for traveling wave solutions of fractional Maccari's system with complex structure, *Alex. Eng. J.*, **79**, (2023) 508–530. https://doi.org/10.1016/j.aej.2023.08.007
22. Z. M. Emad, S. S. M. A. Shehata, M. N. Alam, A. Lanre, Exact propagation of the isolated waves model described by the three coupled nonlinear Maccari's system with complex structure, *Int. J. Modern Phys. B*, **35** (2021), 2150193. https://doi.org/10.1142/S0217979221501939
23. H. U. Rehman, M. A. Imran, N. Ullah, A. Akgul, Exact solutions of (2+1)-dimensional Schrodinger's hyperbolic equation using different techniques, *Numer. Meth. PDE*, **39** (2023), 4575–4594. https://doi.org/10.1002/num.22644
24. D. Jordan, P. Smith, *Nonlinear ordinary differential equations: an introduction for scientists and engineers*, Cambridge: OUP Oxford, 2007.